Tracking and Prediction of Tumor Movement in the Abdomen

Margrit Betke[1], Jason Ruel[1], Gregory C. Sharp[2], Steve B. Jiang[2], David P. Gierga[2] and George T. Y. Chen[2]

1 Computer Science Department, Boston University, Boston, MA, USA
2 Department of Radiation Oncology, Massachusetts General Hospital, Boston, MA, USA

Abstract. Methods for tracking and prediction of abdominal tumor movement under free breathing conditions are proposed. Tumor position is estimated by tracking surgically implanted clips surrounding the tumor. The clips are segmented from fluoroscopy videos taken during pre-radiotherapy simulation sessions. After the clips have been tracked during an initial observation phase, motion models are computed and used to predict tumor position in subsequent frames. Two methods are proposed and compared that use Fourier analysis to evaluate the quasi-periodic tumor movements due to breathing. Results indicate that the methods have the potential to estimate mobile tumor position to within a couple of millimeters for precise delivery of radiation.

1 Introduction

The National Cancer Institute estimates that 8.9 million Americans have a history of cancer in 1999 and more than 1,500 Americans die of cancer per day (Cancer Facts and Figures 2005). In 2005, 253,500 new cases of cancer of the digestive system are expected. The respective 5-year survival rates for cancer of the liver, pancreas, and stomach are 8%, 4%, and 23%. Radiation therapy is an important treatment option that can extend survival and relieve symptoms in many patients.

It is essential in radiation therapy to have accurate knowledge of the position and volume of the tumor to effectively apply sufficient radiation to the tumor while minimizing exposure to the surrounding normal tissue. Treatment is commonly planned in simulation sessions with fluoroscopy, an imaging method in which X-rays strike a fluorescent plate that is coupled to a video monitor. Unfortunately fluoroscopy does not provide a sufficient contrast between abdominal tumors and their surrounding soft tissues, which have similar densities. In preparation of radiation therapy, radio-opaque metal clips are therefore implanted around the tumor. The high-density clips can be observed in the fluoroscopy video as they move with the tumor. The tumors change position and may deform due to various rigid and non-rigid body movements. Respiration, in particular, causes significant internal movements of abdominal tumors. Gierga et al. [12], for example, measured the average magnitude of peak-to-peak tumor motion for seven patients to be 7.4 mm in the cranio-caudal and 3.8 mm in the anterior-posterior direction.

Betke M., Ruel J., C. Sharp G., B. Jiang S., P. Gierga D. and George T. Y. Chen A. (2006).
Tracking and Prediction of Tumor Movement in the Abdomen.
In *6th International Workshop on Pattern Recognition in Information Systems*, pages 27-37
DOI: 10.5220/0002471800270037

After the planning phase is over, radiation therapy is typically performed without concurrent imaging of the tumor. Radiation sessions last several seconds to minutes during which tumor motion is likely to occur. To *prevent* or *reduce* thoracic and abdominal tumor movement, breath-hold and controlled breathing techniques have been proposed [2, 21]. To *compensate* for tumor movements, respiratory-gating and motion-adaptive radiotherapy have been introduced [14, 18, 25]. The idea of the compensating technologies is to operate the radiation beam depending on the tumor position. Gating technology can be used to turn the radiation beam on or off whenever the tumor enters or leaves the field of the beam, respectively. Tracking technology can be used to move the radiation beam with the tumor. The SMART system [18] and the 4-D treatment system [25] are two sample implementations of motion-adaptive radiotherapy techniques.

The appearance of the new technologies reinforces the need for image analysis methods that can accurately determine tumor position in real time *during* the treatment delivery process. For a method to be successful, it must work within the limitations imposed by (1) imaging, (2) computing, and (3) actuating processes: (1) The frame rate of the imaging process directly impacts tracking accuracy, thus a high rate would be desirable. However, when fluoroscopy is used as the imaging tool, patients are exposed to radiation, and therefore a high frame rate cannot be employed. From the radiation safety point of view, the tumor should be imaged as infrequently as possible. (2) For the method to work in real time, the inverse of the frame rate limits the time the method can take to capture a frame, measure tumor position in this frame, and accurately estimate tumor position in subsequent frames. (3) The actuating process causes a latency problem – it takes time to move hardware components and control the radiation beam. The unique frame-rate, processing-time, and latency issues distinguish the tumor tracking problem from other motion estimation problems in computer vision, which typically rely on high frame rates, do not have latency issues, and focus on estimating position in the current frame based on measurements in previous frames, e.g., [8, 9]. The two methods proposed here address the latency problem by estimating the tumor position for a large number of subsequent frames. Prediction accuracy is evaluated by varying parameters such as length of the measurement period, sampling frequency during the measurement period, and length of the prediction period.

The proposed methods model and predict a patient's sinusoidal breathing patterns based on Fourier analysis and least-squares fitting. Analysis of periodic motion can also be found in the study of the cardiovascular system [1, 3, 17] and in human gait analysis, e.g., [6, 7, 15, 16]. Related fields are pattern matching of time series, e.g., [10, 19, 20], and data mining of periodic patterns, e.g., [13]. In radiation oncology, there has been a relatively recent focus on tracking and prediction of tumor motion [5, 14, 18, 22, 24, 25]. Our work is bringing about a connection between these fields by introducing new motion prediction algorithms and applying them to an urgent problem in radiotherapy. Both methods have the potential to facilitate real-time tracking of the tumor motion during the treatment process and allow for precise delivery of radiation dose to moving abdominal tumors.

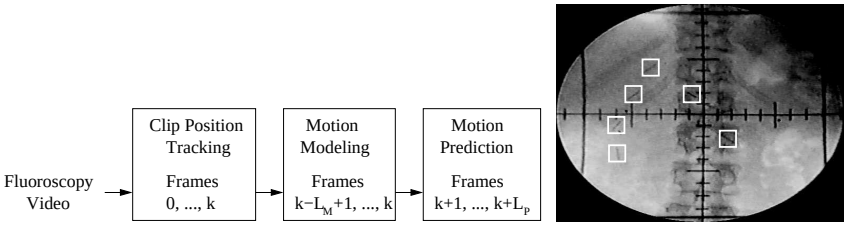

Fig. 1. Left: Problem Overview. Right A fluoroscopy image of an abdominal tumor. The six clips surrounding the tumor are marked by white squares.

2 Clip Tracking and Prediction Methods

An overview of the problem is given in Figure 1, left. The tracking process is performed on each frame of the incoming fluoroscopy video stream. At current frame k, the clip positions in the past L_M image frames are used to model the tumor motion in the modeling phase M. The model is then used to predict the tumor motion in the L_P subsequent frames of prediction phase P. Tracking is initiated by manual selection of a region containing the clip in the first frame of the fluoroscopy video, see Figure 1, right. This region is further processed to isolate the clip from nearby clips that are potentially included in the region. Each isolated clip is then matched and tracked in subsequent frames using a template of a surgical clip. The template T is matched to the image I by maximizing the normalized correlation coefficient. Tracking proceeds by finding the subimage of each subsequent frame that best matches with the template. Breathing is a quasi-periodic, roughly sinusoidal motion. The motion of internal organs due to breathing is poorly understood. In the ideal case, the motion $b(t) = (x(t), y(t), z(t))^T$ of the abdominal tumor is due to regular breathing, i.e., periodic in T, so that $b(t) = b(t+T)$ can be inferred from averaging the three-dimensional motion of its surrounding clips. The motion can then be modeled with a simple sinusoidal waveform, for example,

$$b(t) = m + a\cos(2\pi f t - \psi), \tag{1}$$

describing changes in position in the cranio-caudal direction with amplitude a, frequency $f = 1/T$, phase ψ, and mean position m. With a more general, realistic model, the breathing motion $b(t)$ can be written as an infinite Fourier series

$$b(t) = m + \sum_{n=1}^{\infty} a_n \cos\left(\frac{2\pi n t}{T} - \psi_n\right) \tag{2}$$

in "magnitude-angle form" [26], where T is the period of the signal $b(t) = b(t + T)$, $m = 1/T \int_{t=0}^{T} b(t)dt$ is the mean or "DC" component of $b(t)$, $a_n = \sqrt{b_n^2 + c_n^2}$ the magnitude, $\psi_n = \arctan(\frac{c_n}{b_n})$ the phase offset, $b_n = \frac{2}{T}\int_0^T b(t)\cos\frac{2\pi n t}{T}dt$ and $c_n = \frac{2}{T}\int_0^T b(t)\sin\frac{2\pi n t}{T}dt$. Equation 2 can also be written in terms of multiples of the breathing frequency $f_n = \frac{n}{T}$, which yields $b(t) = m + \sum_{n=1}^{\infty} a_n \cos(2\pi f_n t - \psi_n)$.

The cranio-caudal motion $b(t)$ is measured at discrete points $y[k]$ in time during a finite window L_M (see Section 2). If L_M is chosen as an integral multiple of the

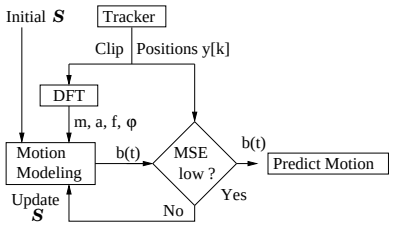

Fig. 2. Clip motion modeling using the shape function approach.

period T (at least approximately), the discrete-time sequence $y[k]$ is periodic in L_M with a discrete Fourier transform (DFT) $Y[n]$ that is periodic in $1/L_M$. The transform pairs are

$$y[k] = \sum_{n=0}^{L_M-1} Y[n] e^{j2\pi kn/L_M} \quad \text{and} \quad Y[n] = \frac{1}{L_M} \sum_{k=0}^{L_M-1} y[k] e^{-j2\pi kn/L_M}. \qquad (3)$$

The power spectrum $|Y[n]|^2$ can be used to analyze the distribution of the frequency coefficients of the data. If there is a strong peak in the power spectrum we may conclude that there is a *dominant frequency* $f_{\max}$ that models the breathing frequency well. This frequency is the $1/T$th frequency coefficient if L_M is a multiple of T and nearby otherwise. The *dominant period* $T_{\max}$ is the inverse of $f_{\max}$. Analysis of the power spectrum helps us determine whether an individual is breathing in a consistent pattern and also whether there is a problem with the system such as jitter in the clip tracking process.

In the following sections we introduce two methods that use Fourier analysis to characterize breathing motion. Both methods model the considerable variations in mean m, amplitude a, and dominant frequency f of tumor motion that we and others, e.g., [18], have observed.

2.1 The Shape-function Approach

We developed a general motion model

$$b(t) = m + a\,\mathbf{S}(\mathbf{\Phi}(t)), \qquad (4)$$

where the *shape* $\mathbf{S}$ is a quasi-sinusoidal function that maps a phase angle $\mathbf{\Phi}(t) = \int_0^t 2\pi f(\tau)d\tau - \psi$ to a position in n-dimensional space, i.e., $\mathbf{S} : [0, 2\pi] \rightarrow \mathcal{R}^n$ with $n = 1, 2$ or 3. In our data, significant motion only occurs in the cranio-caudal direction, so we present our waveform model and prediction algorithm for the case of $n = 1$. Our approach, however, can also be generalized to model the two-dimensional motion of clip position $(x[k], y[k])^T$ in fluoroscopy video. The approach also applies to 1D measurements of air flow [5] and can be generalized to three-dimensional measurements of the breathing motion obtained by the multiple x-ray imaging system described by Shirato et al. [25].

The shape function $\mathbf{S}$ models the trajectory of the tumor over a single breathing cycle. It is used as a *waveform pattern* or *temporal template* that models past movements in order to predict future movements. Figure 2 shows the steps of the modeling process. To obtain the initial motion model $b_1(t)$, the parameters m_1, f_1, ψ_1, and

a_1 are computed from the discrete Fourier transform of the first L_M measurements $y[0], \ldots, y[L_M - 1]$ as described above.

The initial shape function $\mathbf{S}_1$ is assumed to be a sinusoid from 0 to 2π. According to Equation 4, the first motion model is then $b_1(t) = m_1 + a_1 \sin(2\pi f_1 t - \psi_1)$, where the dominant frequency f_1 is chosen instead of the average frequency $f_{av} = 1/t \int_0^t 2\pi f(\tau) d\tau$. The tumor positions predicted for future frames $t+1$ to $t + L_P$ are then $b_1(t+1), \ldots, b_1(t + L_P)$. To obtain a motion model $b_k(t)$ at time k, the previous shape function $\mathbf{S}_{k-1}$ is used as $\mathbf{S}_k$, and the discrete Fourier transform of the last L_M position measurements $y[k - L_M + 1], \ldots, y[k]$ is computed, which yields the parameters a_k, f_k, ψ_k, and m_k:

$$b_k(t) = m_k + a_k \, \mathbf{S}_k(2\pi f_k t - \psi_k). \tag{5}$$

The mean squared error (MSE) between this model $b_k(t)$ and the measurements $y[k - L_M + 1], \ldots, y[k]$ is computed to evaluate the accuracy of the model. If the error is too large, the model is improved by updating the shape function as follows. The most recent measured positions $y[t]$ during a full period $t = k - 1/f_k + 1, \ldots, k$ are combined with an appropriate discretization $\mathbf{S}_k$ to yield

$$\mathbf{S}'_k(\mathbf{\Phi}_k(t)) = \lambda w(t) \, \mathbf{S}_k(\mathbf{\Phi}_k(t)) + (1 - \lambda w(t)) \, y[t], \tag{6}$$

where $\lambda > 0.5$ is a constant that gives the shape function more weight than the measurements and $w(t)$ is an exponential weighting function that gives recent measurements greater weight than earlier measurements. The motion model $b_k(t) = m_k + a_k \, \mathbf{S}'_k(2\pi f_k t - \psi_k)$ is then used to predict the next L_P tumor positions.

2.2 The Half-cycle Approach

The half-cycle approach is an alternative method for predicting abdominal tumor motion. Instead of using a shape function as a temporal template for one breathing cycle, it uses a sinusoid as a template for half a breathing cycle. The approach computes a sequence of sinusoids that models the motion history from the beginning of the video, i.e., $y[0], \ldots, y[k]$, and is used to predict tumor positions $y[k+1], \ldots, y[k + L_P]$. Each sinusoid models the data during an inhalation or an exhalation phase.

We consider the mean m_k of the data $y[0], \ldots, y[k]$ to be the "neutral" position of a clip (or the collection of clips describing the tumor) that it assumes when inhalation changes to exhalation and vice versa. The mean m_k, dominant period T_k, and phase angle ψ_k are obtained by Fourier analysis $y[0], \ldots, y[k]$ as described above. We then subtract m_k from the data so that the clip in the resulting sequence $y_m[0], \ldots, y_m[k]$ is shifted to the ideal position 0 mm. Due to the digitization of time, the neutral position typically occurs at zero crossings in the data. Not all zero crossings, however, correspond to neutral positions because of noise in the measurements. We consider frame t_z to contain a candidate zero crossing if either $y_m[t_z] = 0$ or if there is a sign change from $y_m[t_z - 1]$ to $y_m[t_z]$. Phase ψ_k is used to determine the first frame t_{z_0} with a zero crossing. The frame containing the next zero crossing is located in a small window around $t_{z_0} + T_k/2$. Subsequent zero crossings are found similarly by searching in a window

around the frame index obtained from adding the half of the dominant period to the previous zero crossing. To select a single point among several candidate zero crossings in the same window, we use a non-maximum suppression algorithm [23].

Once the zero crossings have been located, half a cycle of a cosine function is fitted between each pair of crossings. The frequency of the jth cosine template is $f_{k,j} = 1/(2(t_{z_{j+1}} - t_{z_j}))$, the phase is either $\frac{\pi}{2}$ or $\frac{3\pi}{2}$, and the amplitude $a_{k,j}$ is computed using a least squares method:

$$a_{k,j} = \arg\min_{a} \sum_{t=0}^{t_{z_{j+1}} - t_{z_j}} (a\cos[2\pi(t + t_{z_j})f_{k,j} - \psi_{k,j}] - y_m[t + t_{z_j}])^2. \quad (7)$$

The parameters of the resulting j half-cycle cosine functions are then used as models to predict the parameters of the $j+1$st half cycle. In particular, predicted frequency $f_{k,j+1}$ is the weighted average of the frequencies $f_{k,0}, \ldots, f_{k,j}$. Each frequency is weighted by its index so that the most recent breathing pattern is accounted for most. Predicted amplitude $a_{k,j+1}$ is computed similarly from $a_{k,0}, \ldots, a_{k,j}$. Predicted phase $\psi_{k,j+1}$ is $\frac{3\pi}{2}$ if $\psi_{k,j}$ is $\frac{\pi}{2}$ and $\frac{\pi}{2}$ otherwise.

3 Results

The tracking and modeling methods were tested on fluoroscopy video of seven patients obtained under clinical protocol during simulation sessions prior to radiation treatment. The patient names used here are fictitious. The videos contained a total of 23 clips. We verified by visual inspection that the clips were generally tracked reliably.

Radiation exposure time during the fluoroscopy sessions was limited to about seven breathing cycles. The length of the videos ranged from 20 s to 36 s. For five sequences, we were able to test our algorithm with a modeling window length of $L_M = 480$, which corresponded to about four breathing cycles. For the two shorter sequences, we used $L_M = 380$. We evaluated the prediction performance of the motion models for the remaining breathing cycles. To obtain a sample that is sufficiently large for testing, we moved the modeling window $K = 100$ times through the video, each time by one frame. A length of $L_P = 10$ was used for the prediction window.

Prediction accuracy of the motion model at time k is computed by averaging the distances between predicted and eventually measured data points $b(t)$ and $y(t)$ over the length of the prediction window: $E(k) = \frac{1}{L_p}\sum_{t=k}^{k+L_p} |b(t) - y(t)|$. We also compute the prediction accuracy of modeling the motion in a full video by averaging the results obtained for the K motion models tested: $E = \frac{1}{K}\sum_{k=1}^{K} E_p(k)$, where the first prediction $k = 1$ starts at frame $L_M + 1$. The average errors for the seven patients was 1.64 mm using the shape-function approach and 1.04 mm using the half-cycle approach, which is considerably lower. However, the average variance in the error was 0.2 mm^2 for the shape-function approach and 0.85 mm^2 for the half-cycle approach, which is considerably higher. Table 1 shows the motion prediction results in more detail. Examples of successful prediction using the two approaches are shown in Figure 3.

The average and standard deviations of the 100 shape functions are shown in Figure 4 for two patients. The graphs show the signal dependence of the standard deviation

Table 1. Prediction Results with the Shape-function Approach and the Half-cycle Approach.

Patient	No. of Clips	Prediction Error Average in mm		Prediction Error Variance in mm^2		Period in Hz	
		Shape	Cycle	Shape	Cycle	Shape	Cycle
Alice	4	2.62	1.63	0.54	1.66	3.45	3.73
Bob	2	1.75	0.76	0.14	0.25	2.90	2.86
Carol	3	2.81	1.24	0.52	2.14	3.47	3.26
Doug	3	0.78	0.81	0.03	0.66	3.38	3.52
Eve	7	0.90	0.72	0.05	0.42	2.94	3.24
Frank	2	1.69	1.59	0.05	0.73	3.38	3.53
Gary	2	0.90	0.52	0.03	0.07	3.19	2.88

of the shape model. In particular, the position model deviates more for phase angles corresponding to inspiration than expiration. This indicates that our breathing prediction in the direction of the cranium is more reliable than in the caudal direction.

The methods' prediction accuracy over longer prediction windows was tested for patient Eve. Eve's video is the longest among the videos and allowed us to test $K = 260$ predictions. The error for the prediction window lengths $L_P = 1, \ldots, 120$ is shown in Figure 5, top, for the two methods. We also evaluated the prediction accuracy of motion models that were computed over modeling windows with the same length but sparser sampling. Figure 5, bottom, shows the average prediction error when the output of the tracker is sampled at a rate of $30/j$ Hz for $j = 1, 2, \ldots, 15$. The average errors for sampling rates 10 Hz, 15 Hz, and 30 Hz are approximately the same.

4 Discussion and Conclusions

We have introduced two motion modeling and prediction methods for tracking abdominal tumor movement. With average errors of 1.64 mm and 1.04 mm, the motion prediction methods appear to model the tumor movement rather well. Our goal is to eventually reduce the error to less than 1 mm in order to facilitate real-time tracking of the tumor motion during the treatment process and allow for precise delivery of radiation dose to mobile tumors.

In future work, we will examine whether a combination of the two approaches results in more accurate modeling and prediction performance. The zero-crossing analysis in the half-cycle approach may serve to verify the frequency and phase estimation in the shape function approach. Longer training times may improve prediction performance. Longer sequences may be obtained without exposing patients to additional radiation by tracking external markers that are placed on the patient's abdomen with a visible-light or infra-red video camera. Preliminary results [11] suggest that there is a correlation between the motion of the clips and such external markers. Our goal is to lower the frame rate as much as possible to limit the imaging radiation dose delivered to the patient. Our preliminary results indicate that a frame rate of 30 Hz may not be necessary for reliable prediction of breathing motion. While both methods maintain low error rates in the sampling experiment, more testing is needed to evaluate tracking performance at reduced frame rates.

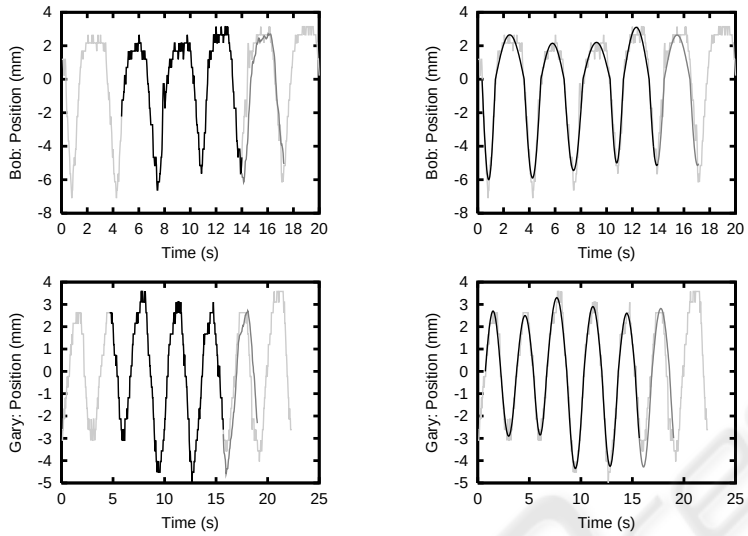

Fig. 3. Position prediction results for Bob (top) and Gary (bottom) using the shape-function approach (left) and the half-cycle approach (right). The output from the tracker is shown in light gray, the training period L_m for the shape-function approach and the fitted sinusoids in the half-cycle approach respectively in black, and the predicted positions in dark gray.

In addition to accuracy, ease of use is crucial for a new technology to become applicable to the clinical environment. With current technology, complete patient setup and treatment in a busy clinic typically fit within a 15-minute appointment. Our algorithms are therefore incorporated into an easy-to-use computer interface. A human operator can use a single mouse click to select the image region that contains the clip in the initial frame. The remaining tracking, modeling, and prediction processes are then computed automatically.

For our future motion-adaptive radiotherapy system, we plan to use frame buffering to store the images acquired while the operator selects the clips in the initial frame. During this period, the patient keeps breathing and the clips move. The tracker must analyze the buffered frames and then catch up to the incoming frames so that the clip positions are tracked in real time.

Acknowledgements

Funding was provided by The Whitaker Foundation, the National Science Foundation (IIS-0093367, P200A01031, and EIA-0202067), and the Office of Naval Research (N000140110444).

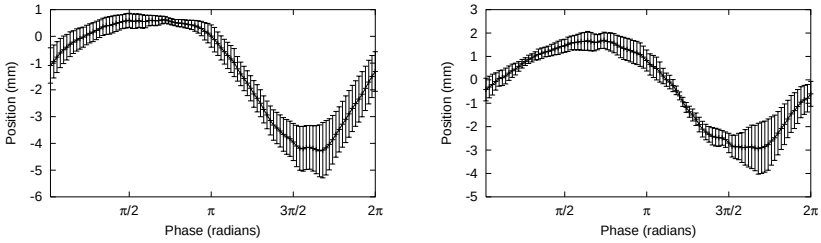

Fig. 4. The average shape function and its standard deviation is computed over $K = 100$ models for one of the clips of patient Bob (left) and of patient Doug (right).

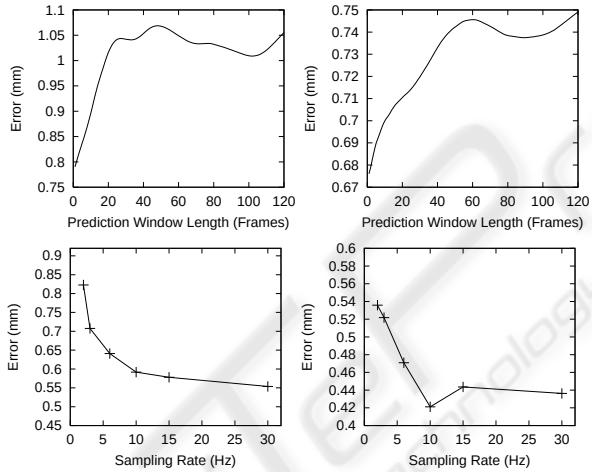

Fig. 5. Error in predicting tumor motion of patient Eve as a function of the length of the prediction window L_P (top) and sampling frequency (bottom) for the shape-function approach (left) and the half-cycle approach (right).

References

1. Ashkenazy, Y, Ivanov, PC, Peng, SH CK, Goldberger, AL, and Stanley, HE (2001). Magnitude and sign correlations in heartbeat fluctuations. *Phys Rev Lett*, 86(9):1900–1903.
2. Balter, JM, Lam, KL, McGinn, CJ, Lawrence, TS, and Haken, RKT (1998). Improvement of CT-based treatment planning models of abdominal targets using static exhalation imaging. *Int J Radiat Oncol Biol Phys*, 41(4):939–943.
3. Bettermann, H, Cysarz, D, and Leeuwen, PV (2002). Comparison of two different approaches in the detection of intermittent cardioresperatory coordination during night sleep. *BMC Physiology*, 4(2):1–18.
4. Cancer Facts and Figures 2005, American Cancer Society. http://www.cancer.org.
5. Chen, QS, Weinhous, MS, Deibel, FC, Ciezki, JP, and Macklis, RM (2001). Fluoroscopic study of tumor motion due to breathing: facilitating precise radiation therapy for lung cancer patients. *Med Phys*, 28(9):1850–1856.

6. Collins, RT, Gross, R, and Shi, J (2002). Silhouette-based human identification from body shape and gait. In *Proceedings of the 5th IEEE International Conference on Automatic Face and Gesture Recognition*, pages 366–371, Washington, DC.
7. Cutler, R and Davis, L S (2000). Robust periodic motion and motion symmetry detection. In *Proceedings of the IEEE Conference on Computer Vision and Pattern Recognition*, pages 2615–2622, Hilton Head Island, SC.
8. Fagiani, C, Betke, M, and Gips, J (2002). Evaluation of tracking methods for human-computer interaction. In *Proceedings of the IEEE Workshop on Applications in Computer Vision*, pages 121–126, Orlando, FL.
9. Forsyth, DA and Ponce, J (2003). *Computer Vision, A Modern Approach, pp. 373–398*. Prentice Hall, NJ.
10. Ge, X and Smyth, P (2000). Deformable Markov model templates for time-series pattern matching. In *Proceedings of the Sixth ACM SIGKDD International Conference on Knowledge Discovery and Data Mining*, pages 81–90, Boston, MA.
11. Gierga, DP, Chen, GTY, Kung, JH, Betke, M, Lombardi, J, Willett, CG (2004). Quantification of respiration-induced abdominal tumor motion and its impact on IMRT dose distributions. *Int J Radiat Oncol Biol Phys*, 58(5):1584–1595.
12. Gierga, DP, Brewer, J, Sharp, GC, Betke, M, Willett, CG, Chen, GTY (2005). The correlation between internal and external markers for abdominal tumors: implications for respiratory gating. *Int J Radiat Oncol Biol Phys*, 61(5):1551–1558.
13. Indyk, P, Koudas, N, and Muthukrishnan, S (2000). Identifying representative trends in massive time series data sets using sketches. In *Proceedings of the 26th International Conference on Very Large Databases (VLDB'00)*, pages 363–372, Cairo, Egypt.
14. Keall, PJ, Kini, VR, Vedam, SS, and Mohan, R (2001). Motion adaptative x-ray therapy: a feasibility study. *Phys Med Biol*, 46(1):1–10.
15. Lee, L and Grimson, WEL (2002). Gait analysis for recognition and classification. In *Proceedings of the 5th IEEE International Conference on Automatic Face and Gesture Recognition*, pages 155–162, Washington, DC.
16. Little, JJ and Boyd, JE (1998). Recognizing people by their gait. *Videre*, 1(2):1–32.
17. Lotric, MB and Stefanovska, A (2000). Syncronization and modulation in the human cardiorespiratory system. *Physica A*, 286:451–461.
18. Neicu, T, Shirato, H, Seppenwoolde, Y, and Jiang, SB (2003). Synchronized Moving Aperture Radiation Therapy (SMART): Average tumor trajectory for lung patients. *Phys Med Biol*, 48(5):587–598.
19. Noone, G and Howard, S (1995). Investigation of periodic time series using neural networks with adaptive error thresholds. In *Proceedings of the International Conference on Neural Networks (ICNN)*, pages 1541–1545, Western Australia.
20. Oates, T, Firoiu, L, and Cohen, PR (1999). Clustering time series with hidden Markov models and dynamic time warping. In *IJCAI'99 Workshop on Neural, Symbolic, and Reinforcement Methods for Sequence Learning*, 5 pages, Stockholm, Sweden.
21. Rosenzweig, KE, Hanley, J, Mah, D, Mageras, G, Hunt, M, Toner, S, Burman, C, Ling, CC, Mychalczak, B, Fuks, Z, and Leibel, SA (2000). The deep inspiration breath-hold technique in the treatment of inoperable non-small-cell lung cancer. *Int J Radiat Oncol Biol Phys*, 48(1):81–87.
22. Schweikard, A, Glosser, G, Bodduluri, M, Murphy, MJ, and Adler, JR (2000). Robotic motion compensation for respiratory movement during radiosurgery. *Comput Aided Surg*, 5(4):263-277.
23. Shapiro, L G and Stockman, G C (2001). *Computer Vision, page 299*. Prentice Hall, NJ.
24. Shirato, H, Shimizu, S, Kitamura, K, Nishioka, T, Kagei, K, Hashimoto, S, Aoyama, H, Kunieda, T, Shinohara, N, Dosaka-Akita, H, and Miyasaka, K (2000). Four-dimensional

treatment planning and fluoroscopic real-time tumor tracking radiotherapy for moving tumor. *Int J Radiat Oncol Biol Phys*, 48(2):435–442.

25. Shirato, H, Shimizu, S, Kunieda, T, Kitamura, K, van Herk, M, Kagei, K, Nishioka, T, Hashimoto, S, Fujita, K, Aoyama, H, Tsuchiya, K, Kudo, K, and Miyasaka, K (2000). Physical aspects of a real-time tumor-tracking system for gated radiotherapy. *Int J Radiat Oncol Biol Phys*, 48(4):1187–1195.
26. Siebert, W (1986). *Circuits, Signals, and Systems*. MIT Press.